ACS OMEGA

Article

Cite This: ACS Omega 2019, 4, 5335−5344

http://pubs.acs.org/journal/acsodf

Inhibiting S100B($\beta\beta$) for Activating Wild-Type p53: Design of Stapled Peptides

Srinivasaraghavan Kannan,*[,†] Pietro G. A. Aronica,[†] Yaw Sing Tan,[†] and Chandra S. Verma*[,†,‡,§]

[†]Bioinformatics Institute, Agency for Science, Technology and Research (A*STAR), 30 Biopolis Street, #07-01 Matrix, 138671 Singapore

[‡]School of Biological Sciences, Nanyang Technological University, 60 Nanyang Drive, 637551 Singapore

[§]Department of Biological Sciences, National University of Singapore, 14 Science Drive 4, 117543 Singapore

Supporting Information

ABSTRACT: S100B($\beta\beta$) is a member of the S100B protein family and is distributed in a cell-specific manner. Its levels are elevated in several cancers such as malignant melanoma and correlate directly with poor prognosis in patients. S100B($\beta\beta$) directly interacts with the tumor suppressor p53, inhibiting tetramerization and protein kinase C-dependent phosphorylation, consequently decreasing p53 DNA binding and transcriptional activity, and preventing apoptosis. Thus, S100B($\beta\beta$) is being pursued as a target for therapeutic inhibition. However, development of small molecule inhibitors targeting p53-interactions has met with limited success. In this work, we present a set of designed stapled peptide inhibitors of S100B($\beta\beta$), guided by the structure of the C-terminal domain of p53 complexed with S100B($\beta\beta$). We further modified a tightly binding stapled peptide with imaging agents and propose these as potential diagnostic agents to detect S100B($\beta\beta$) as a biomarker.

INTRODUCTION

The S100 protein family is a highly conserved group of Ca^{2+}-binding proteins consisting of more than 20 family members that are named after their solubility in 100% ammonium sulfate. They are regulators of protein−protein interactions (PPIs), acting as calcium-activated switches, similar to calmodulin.[1] These proteins are involved in calcium homeostasis, cell−cell communication, cell proliferation, differentiation, cytoskeletal dynamics, cell morphology, etc.[2−5] One of the most extensively studied members is S100B($\beta\beta$), a symmetric homodimer, found both intra- and extracellularly.[2,3,6,7] The solution structure of the apo-S100B($\beta\beta$) shows that the two subunits associate through extensive hydrophobic interactions to form a compact dimer with a highly charged surface;[8−12] each subunit of S100B($\beta\beta$) contains four α helices (Figure 1). S100B($\beta\beta$) is known to interact with several proteins as part of multiple pathways and cellular functions.[13] It is increasingly becoming apparent that S100B($\beta\beta$) can increase proliferation and migration and suppress differentiation and apoptosis.[14−16] S100B($\beta\beta$) regulates the transcriptional activity of p53 by binding to its C terminal[17−20] and can prevent apoptosis, as has been shown, for example, in melanoma cells.[18−26] Inhibition of Ca-bound S100B($\beta\beta$) has been shown to reactivate p53[21−23] and has been pursued as a therapeutic target against cancer.[24−27] Pentamidine, an Food and Drug Administration (FDA)-approved drug, was one of the early inhibitors of S100B($\beta\beta$).[28,29] However, its undesirable toxicity[30−32] prompted efforts to improve its safety.[30−33] In addition, there are several other ongoing efforts to target S100B($\beta\beta$).[34,35] In general, development of small molecules against interfaces that characterize protein−protein interactions (PPIs) is fraught with difficulties largely because these regions are generally large and flat (in contrast to the deep cavities that typically bind small molecules, 300−500 A^2).[36,37] However, more recently, the discovery of "hot spot" regions at the interfaces (regions that contain most of the interactions) of several PPIs has resulted in the successful development of molecules targeting these PPIs.[36,37] In parallel, peptides and peptidomimetics are increasingly being shown to be efficient inhibitors of PPIs.[38] Their specificity, high biocompatibility, and low toxicity profiles have made them desirable therapeutics. Several hundred peptide and peptidomimetic candidates have advanced into clinical trials for a wide range of therapeutic indications with more than 60 already approved by the FDA. Their use is limited by proteolytic sensitivity, cellular entry, and low conformational stability, which reduces their affinity and bioavailability.[39,40] A variety of chemical modifications have been explored to overcome some of these issues including cyclization and backbone modifications.[41−44] The main aim of cyclization is to constrain the conformation of the peptide into a bound conformation. One such method that has been gaining popularity is stapling,[43] which has been particularly useful in stabilizing peptides that are required to adopt an α-helical structure in their bound states. Stapling requires the suitable placement of two unnatural amino acids that are then covalently linked by ring closing metathesis or

Received: January 11, 2019
Accepted: March 4, 2019
Published: March 14, 2019

DOI: 10.1021/acsomega.9b00097
ACS Omega 2019, 4, 5335−5344

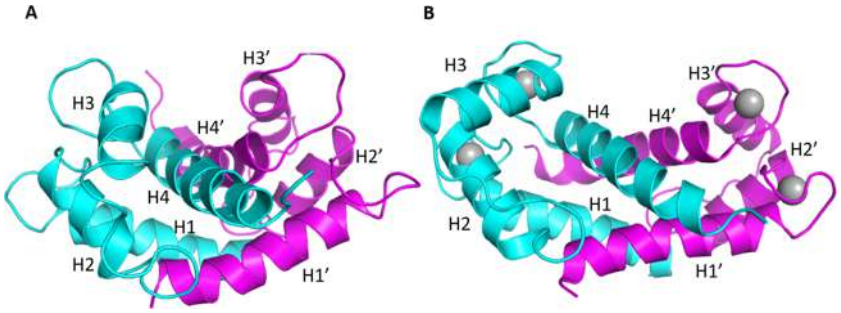

Figure 1. Cartoon representation of (A) apo and (B) calcium-bound conformations of S100B($\beta\beta$) protein. Each monomer in the dimer is colored separately, and the bound calcium is highlighted in gray spheres.

click chemistry. The linkers can be varied as can the separation between the two amino acids (such as $i,i+3$, $i,i+4$, $i,i+7$, $i,i+11$, etc.). In some cases, stapling has resulted in improved cellular penetration.[41,43,44] Although stapling has largely found success in stabilizing α helical peptides, more recently it has found some success in nonhelical peptides too.[45] Examples of successful PPI inhibition include p53−MDM2 BCL-2 family−BH3 domains, β-catenin−TCF, Rab−GTPase-effector, ERα−coactivator protein, cullin3−BTB, VDR−coactivator protein, and β-arrestin−β-adaptin.[45] A stapled peptide inhibitor of HDM2/HDMX toward the activation of p53 is currently in phase II clinical trials.[46]

The solution structure of a peptide from the C terminus of p53 (p53CTD) complexed to S100B($\beta\beta$) shows that the peptide in an α-helical conformation.[47] We exploit this toward the computational design and development of a set of stapled peptide inhibitors of S100B($\beta\beta$) aimed at disrupting the S100B($\beta\beta$)−p53 interaction.

RESULTS

Conformational Dynamics of Apo and S100B($\beta\beta$)-Bound p53CTD. A peptide from the C-terminal domain (CTD) of p53 (residues 367−388) has been shown to bind to the S100B($\beta\beta$) receptor, adopting an α-helical conformation from residues 376 to 388 (sequence, STSRHKKLMFKTE); the region 367−375 is highly disordered and does not engage in any specific interaction with the S100B($\beta\beta$) protein (Figure S1).[47] In the available NMR structure (PDB ID: 1dt7),[47] a single p53CTD peptide is bound to each monomer of the S100B($\beta\beta$) dimer and each peptide interacts with only one of the monomers of S100B($\beta\beta$) (Figure 2). The binding site is relatively large, with SASA ~3 nm^2, and is mainly hydrophobic, surrounded by negatively charged residues (Figure 2). The binding of the peptide is mostly stabilized by hydrophobic interactions between Leu386 from the peptide and Met79, Val80, Leu44, and Val56 of S100B($\beta\beta$). In addition, electrostatic complementarity/salt bridges between the peptide (Arg4, Lys11) and the receptor (Glu44, Glu45, and Glu86) further stabilize the complex.

Since the region 367−375 of the p53CTD is not involved in any interaction with the S100B($\beta\beta$) protein, we exclude this region in our study. We first carried out molecular dynamics (MD) simulations on the truncated form of the p53CTD peptide (residues 376−388). Since the peptides do not interact with each other, our system had one peptide bound to one monomer in a dimeric construct of S100B($\beta\beta$) (one monomer remained unoccupied). These residues (from 376 to 388) of p53CTD will be numbered 1−13 in the rest of the article. During the MD simulations, the S100B($\beta\beta$)−p53CTD

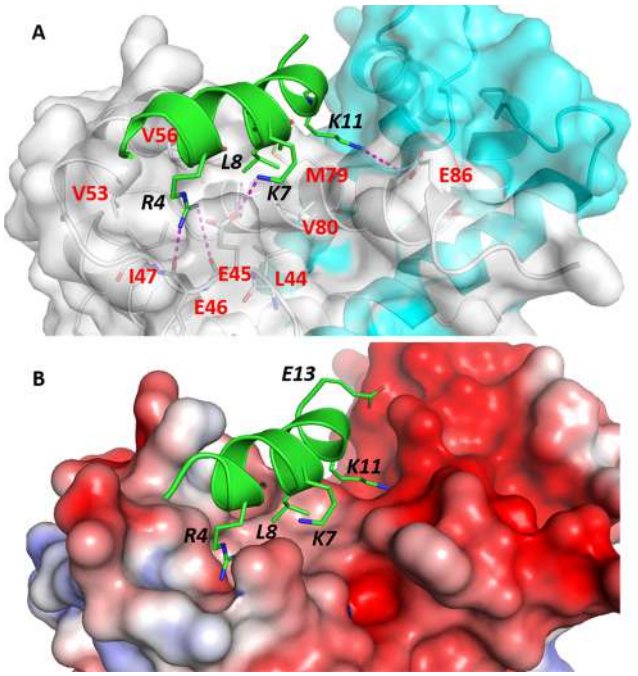

Figure 2. Structure of p53CTD-bound S100B($\beta\beta$) complex. (A) S100B($\beta\beta$) protein dimer is shown as a surface with the two monomers colored separately. The bound peptide is shown as a cartoon (green), and peptide−protein interacting residues and h-bond interactions are highlighted in sticks and dashed lines, respectively. (B) Electrostatics surface representation (red and blue colors represent electrostatic potentials ranging from −5 to +5 kcal/mol) of the S100B($\beta\beta$) protein dimer with the bound peptide is shown as a green cartoon with interacting residues from the peptide highlighted in sticks.

(truncated) complex remained stable with no unbinding of peptide observed. The S100B($\beta\beta$) dimer remained stable with root-mean-square deviation (RMSD) below ~3.5 Å from the experimental structure (Figure 3). The bound p53CTD showed increased flexibility arising from the increased flexibility of long and flexible side chain residues of the peptide that are involved in interactions with the solvent-exposed side chains from S100B($\beta\beta$). We next investigated the conformational dynamics of the apo-S100B($\beta\beta$) protein and p53CTD peptide in solution. The apo-S100B($\beta\beta$) dimer remained stable with RMSD within ~3.5 Å of the crystal structure (Figure 3), but the apo p53CTD is less stable in solution. In solution, apo p53CTD rapidly lost its α-helical structure and was seen to be highly flexible (RMSD > 6 Å against its bound helical conformation (Figure 3)). The apo

DOI: 10.1021/acsomega.9b00097
ACS Omega 2019, 4, 5335−5344

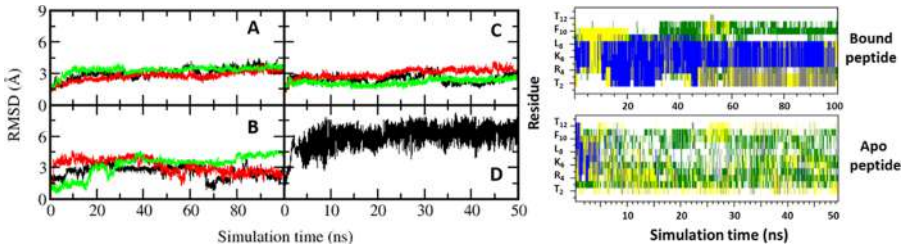

Figure 3. (Left) root-mean-square deviation (RMSD) of (A, C) S100B($\beta\beta$) and (B, D) p53CTD in bound (A, B) and apo states (C, D). In the case of the complex (A, B) and apo-S100B($\beta\beta$) (C), all of the conformations sampled during standard MD simulations and in the case of the apo peptide (D) conformations sampled during the biasing potential-replica-exchange molecular dynamics (BP-REMD) simulations were used for RMSD calculations against the corresponding starting structure. (Right) time evolution of the secondary structure of the S100B($\beta\beta$)-bound and apo peptide conformations sampled from the standard MD and BP-REMD simulations, respectively.

peptide mostly samples disordered states with only ~8% α helicity (Figure 3). The solution behavior of p53CTD has been shown by circular dichroism and NMR to be unfolded or disordered.[47,48]

This suggests that constraining the peptide in a conformation that resembles its bound α-helical conformation may result in high-affinity binders.[41,44] To test this hypothesis, we design a set of stapled peptides of the p53CTD to constrain it in an α-helical conformation.

Design of Stapled Peptides. We first identify residues in the peptide that are not critical for binding to S100B($\beta\beta$) and can be replaced by amino acids necessary for stapling. We mine the MD simulations of the complex of p53CTD (1−13) to examine the contributions of each residue of the peptide to the total binding energy. It is clear from the per-residue energy decomposition analysis that residues Arg4, Lys6, Lys7, Leu8, Phe10, and Lys11 contribute favorably to binding, with Arg4 contributing the most (Figure 4). The residue Glu13 at the C terminus of the peptide does not contribute favorably, whereas the remaining residues make negligible interactions. The contribution of peptide residues was additionally explored by carrying out in silico alanine scanning in which each peptide residue is mutated to alanine in each conformation of the MD simulation, and the change with respect to the binding energy of the wild-type peptide is calculated using molecular mechanics Poisson−Boltzmann surface area (MMPBSA). As expected, the in silico alanine scanning results mirrored the decomposition analysis with major losses in affinity observed for Arg4 and additionally for Lys6, Lys7 leu8, Phe10, and Lys11 (Figure 4). Interestingly, the substitution of Glu13 with Ala results in favorable binding, whereas the remaining residues are agnostic to substitution with alanine; this is not surprising as Glu13 is surrounded by negatively charged amino acids in S100B($\beta\beta$) (Figure 2B). Based on these observations, we next designed a set of 15 stapled peptides stapled across residues $i,i+3$, $i,i+4$, or $i,i+7$ (listed in Figure 5).

Peptide Stapling Increases Helicity of Apo p53CTD. MD simulations were carried out on the stapled peptides in solution starting from the bound α-helical conformation. To enhance the sampling of the peptide conformations, Hamiltonian replica-exchange molecular dynamics (HREMD), a method commonly used and found to produce data in accord with experiments, was used. Whereas the linear wild-type peptide was mostly disordered in solution (<10% α helicity) as expected, the stapled peptides displayed varying degrees of helicity, ranging from 17 to 46% (Figures 5 and 6). A caveat is that although stapling has been shown to result in increased helicity in general,[49] it is also a function of the

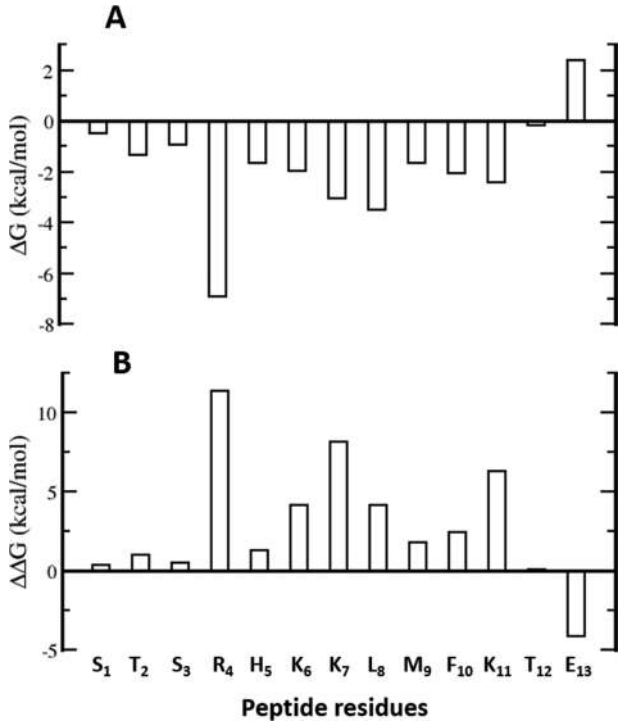

Figure 4. Energetic analysis of the MD simulations of the S100B($\beta\beta$)−p53CTD complex. (A) Binding free energy contributions of p53CTD peptide residues to the total interaction energy with S100B($\beta\beta$). (B) Computational alanine scanning of p53CTD peptide residues.

position of the staple and the nature of the amino acids and increased helicity does not necessarily correlate with increased affinity.[49] Most of the peptides designed displayed a moderate increase in helicity (>30%). Analysis of residue-wise helicity revealed that the stapled peptides retain helicity largely in the centers of the peptides, whereas the termini display increased flexibility; no correlation was apparent between changes in helicity and the position of the staples.

Modeling of the S100B($\beta\beta$)−Stapled p53CTD Peptide Complex. We next modeled the complexes between the stapled peptides and the S100B($\beta\beta$) (dimer). We adopted a simple scheme of introducing staples in the peptides in their complexed states (based on the crystal structure) and subjected the 15 complexes to MD simulations in triplicates for 100 ns. Unsurprisingly, all of the modeled complexes remained stable, with no unbinding events observed for any of the peptides. The peptide bound conformation of the

DOI: 10.1021/acsomega.9b00097
ACS Omega 2019, 4, 5335−5344

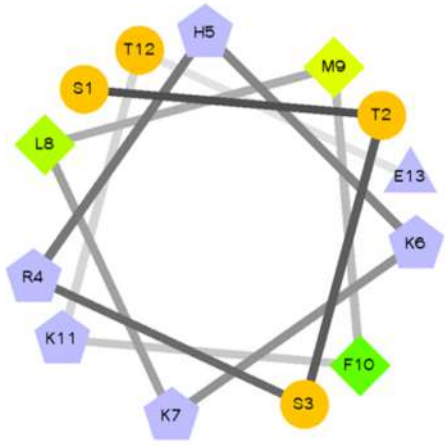

Peptide	Sequence														
		1	2	3	4	5	6	7	8	9	10	11	12	13	
WT	Ac-	S	T	S	R	H	K	K	L	M	F	K	T	E	NH2
Spep1	Ac-	S	T	*R5*	R	H	*S5*	K	L	M	F	K	T	E	NH2
Spep2	Ac-	S	T	S	R	H	*S5*	K	L	M	*S5*	K	T	E	NH2
Spep3	Ac-	S	T	S	R	H	K	*R5*	L	M	*S5*	K	T	E	NH2
Spep4	Ac-	S	T	*R8*	R	H	K	K	L	M	*S5*	K	T	E	NH2
Spep5	Ac-	S	T	S	R	*R8*	K	K	L	M	F	K	*S5*	E	NH2
Spep6	Ac-	S	T	S	R	*S5*	K	K	L	*S5*	F	K	T	E	NH2
Spep7	Ac-	S	*R5*	S	R	*S5*	K	K	L	M	F	K	T	E	NH2
Spep8	Ac-	S	T	S	R	H	*R8*	K	L	M	F	K	T	*S5*	NH2
Spep9	Ac-	S	T	S	R	H	K	K	L	*S5*	F	K	T	*S5*	NH2
Spep10	Ac-	*S5*	T	S	R	*S5*	K	K	L	M	F	K	T	E	NH2
Spep11	Ac-	S	*S5*	S	R	H	*S5*	K	L	M	F	K	T	E	NH2
Spep12	Ac-	S	*R8*	S	R	H	K	K	L	*S5*	F	K	T	E	NH2
Spep13	Ac-	S	T	*S5*	R	H	K	*S5*	L	M	F	K	T	E	NH2
Spep14	Ac-	S	T	S	R	H	*R5*	K	L	*S5*	F	K	T	E	NH2
Spep15	Ac-	S	T	S	R	H	K	K	L	*R5*	F	K	*S5*	E	NH2

Figure 5. Helical wheel representation of the p53CTD peptide template sequence used for the design of stapled peptides. Sequences of the designed stapled p53CTD peptides are shown here. Residues that are linked through all hydrocarbon linkers *i,i* + 3, *i,i* + 4, and *i,i* + 7 are highlighted in red.

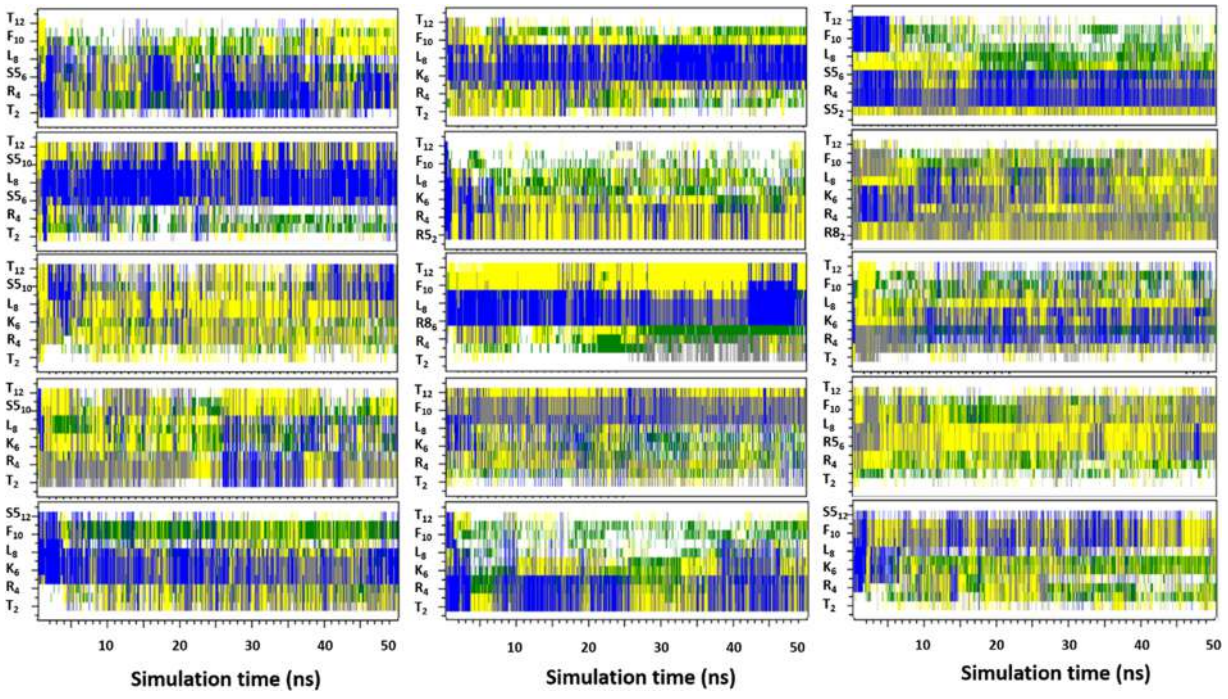

Figure 6. Time evolution of the secondary structures of the designed stapled peptides (from Spep1 to Spep15: first column represents peptides S1−S5 from top to bottom; second column represents peptides S6−S10 from top to bottom; and third column represents peptides S11−S15 from top to bottom) free in solution. The peptide conformations sampled during BP-REMD simulations were used for secondary structure calculations.

S100B($\beta\beta$) dimer was stable with RMSD reaching 3−4 Å from the corresponding starting conformations (Figure 7). Interestingly, the bound stapled peptides displayed increased flexibility, with RMSD values reaching as high as 7 Å (Figure 7); the average RMSD was 4.5 Å, which is slightly higher compared to that of the unstapled peptide. The increased flexibility of the peptide arises from the introduction of hydrocarbon linkers, and the staples do induce greater helicity in the bound peptides compared to the bound linear forms.

Peptide Stapling Increases Binding. We next investigated the effect of stapling on the energetics of interactions of the peptides with S100B($\beta\beta$) using the MMPBSA approach across the MD trajectories. Although this method is fraught with approximations, nevertheless, it has been used successfully to rationalize relative differences in binding affinities.[S0,S1] Binding free energies were calculated using a single trajectory approach in which energies of the complex and of the individual peptide and protein monomers extracted from the complex were used. Energies from the apo simulations of the

DOI: 10.1021/acsomega.9b00097
ACS Omega 2019, 4, 5335−5344

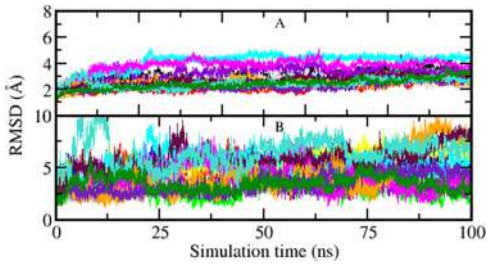

Figure 7. Root-mean-square deviation (RMSD) of (A) S100B($\beta\beta$) and (B) stapled peptides, in bound states. There are too many colors since there are 15 peptides; this graph is only meant to demonstrate that the protein and peptides are structurally stable during the simulations.

peptides and protein monomers were not considered for two main reasons: (1) the peptides in solution are highly flexible with α helicity of only ∼9%. Even upon stapling, the helicity increases only to 17−46%, thus giving rise to large fluctuations in the energies of the various conformations sampled. (2) Upon binding, the peptides adopt >90% helicity. This suggests that entropy must be quite important in the binding. However, it is not expected to converge in the calculations and hence is beyond the scope of the current study. Most of the stapled peptides displayed increased binding compared to that of the linear form, with the improvements in binding energies ranging from 2 to 5 kcal/mol (Figure 8), driven by both van der Waals

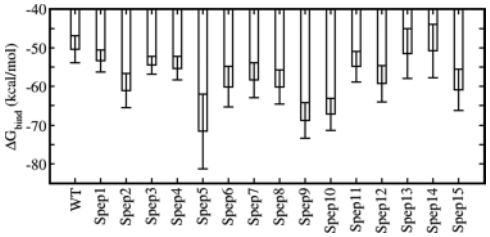

Figure 8. Energetic analysis of the MD simulations of the S100B($\beta\beta$)−stapled peptide complexes. Binding free energy of the interaction of S100B($\beta\beta$) with each stapled peptide was calculated using the MMPBSA approach (see the Materials and Methods section) using the conformations sampled during the MD simulations of the S100B($\beta\beta$)−stapled peptide complexes.

and electrostatic interactions. Residues Arg4, His5, Lys7, Leu8, and Lys11 contribute most to the binding in all of the stapled peptides designed here (Table 1). The unfavorable contribution from Glu13 persists across all the designed peptides except for Spep8 and Spep9 where the replacement of Glu13 by a hydrocarbon linker results in favorable contributions for binding. As expected, the contributions from the hydrocarbon linkers is not uniform with negligible contributions in some cases (Spep1, Spep2, Spep3, Spep4, and Spep13), whereas contributions of >2 kcal/mol are seen in the rest (Table 1). In summary, we have designed a set of stapled peptides that bind S100B($\beta\beta$) dimers with affinities that are as good if not better than the linear peptide.

In Silico Amino Acid Scan for Increased Potency. We next wondered how we could design stapled peptides with much more improved binding affinities for S100B($\beta\beta$). We decided to explore their optimization through point mutations of the wild-type peptide. Using an in silico mutagenesis method called Parasol,[52] all 19 amino acid substitutions were introduced at each position of the peptide in its complex, subject to 100 ns MD simulations (in triplicate for each mutation), and examined for improvements in affinities. All of the simulated complexes remained stable, and no unbinding was observed. As expected, different flexible patterns were observed depending on the kind of mutations introduced at various positions (Figures S2 and S3). For example, substitution of buried or interfacial peptide residues with large and bulkier amino acids such as Arg, Lys, and Trp resulted in increased flexibility, whereas the same substitutions at the exposed sites were well tolerated structurally. Similarly, substitution of Arg4, Lys6, Lys7, and Lys11 with shorter amino acids resulted in increased flexibility as the substitutions resulted in the loss of specific interactions between the peptide and the receptor. Binding free energies of each mutant peptide were estimated by subjecting the simulated conformations to MMPBSA estimates (Figure 9). Residues Arg4, Lys6, Lys7, Leu8, and Lys11 are least tolerable to any substitution, suggesting the importance of the charged residues at these positions. Ser1, Thr2, Ser3, His5, Phe10, and Thr12 can tolerate changes. Glu13, which disfavors binding, tolerates any change except to Asp and is particularly favorable to charge reversal, i.e., Arg or Lys. These calculations recapitulate our earlier observations of the role of important residues.

Table 1. Per-Residue Decomposition Energies of Each S100B($\beta\beta$)−Stapled Peptide Complexes Calculated by MMPBSA[a]

	WT	Spep1	Spep2	Spep3	Spep4	Spep5	Spep6	Spep7	Spep8	Spep9	Spep10	Spep11	Spep12	Spep13	Spep14	Spep15
Ser	−0.5	−0.3	−1.0	−1.5	−0.5	−2.0	−1.2	−0.7	−0.8	−0.5	**−2.2**	−0.2	−0.1	−0.1	0.1	−0.1
Thr	−1.3	−0.4	−2.3	−1.3	−0.7	−0.7	−0.9	**−1.1**	−0.6	−1.1	0.4	**−1.6**	−3.6	−0.4	0.1	−0.9
Ser	−1.0	**−0.1**	−1.0	−0.5	**−0.1**	−0.1	0.2	0.3	0.3	0.2	−0.1	0.1	0.3	**−0.9**	0.1	0.1
Arg	−7.0	−8.3	−9.2	−10.3	−7.9	−10.4	−8.6	−7.1	−5.5	−8.5	−8.5	−7.1	−7.9	−7.4	−9	−8.4
His	−1.7	−2.2	−2.2	−0.7	−1.4	**−7.1**	**−4.1**	**−3.0**	−3.2	−0.9	**−3.2**	−2.3	−0.5	−2.6	−3.6	−2.2
Lys	−2.0	**−0.2**	**−0.4**	−2.7	−2.5	−2.4	−2.1	−2.4	**−0.9**	−1.6	−2.1	−1.2	−1.5	−1.9	**−1**	−1.8
Lys	−3.0	−3.7	−3.0	**−0.8**	−4.2	−3.2	−3.4	−3.0	−2.1	−3.9	−3.8	−2.3	−2	**−0.8**	−2.3	−2.6
Leu	−3.5	−3.8	−4.4	−3.8	−4.5	−2.7	−3.7	−4.1	−2.4	−3.2	−3.2	−2.5	−2.7	−2	−1.8	−3.3
Met	−1.7	−3.9	−3.5	−1.9	−2.8	−1.9	**−3.4**	−2.3	−3.6	**−2.0**	−2.4	−3.6	**−3.8**	−2.7	**−2.5**	**−2**
Phe	−2.1	−1.3	**−0.3**	**−0.3**	**−0.2**	−0.1	−0.3	−1.3	−0.1	−1.6	−1.8	−0.6	−0.4	−2.1	−1.4	0.2
Lys	−2.5	−1.8	−3.8	−1.3	−2.1	−1.9	−2.9	−3.1	−1.8	−2.2	−1.6	−1.8	−1.3	−2.6	−2.3	−1.9
Thr	−0.2	−1.2	−1.9	−1.4	−1.3	**−4.2**	−1.9	−0.7	−0.7	−1.0	−0.7	−1.3	−1.3	−0.1	−0.8	**−4.1**
Glu	2.4	2.5	2.9	3.1	2.5	2.7	4.1	3.3	−1.3	**−1.2**	3.2	3.9	2.8	2.9	2.9	3.5

[a]Values in bold refers to the contribution from the staple linkers.

DOI: 10.1021/acsomega.9b00097
ACS Omega 2019, 4, 5335−5344

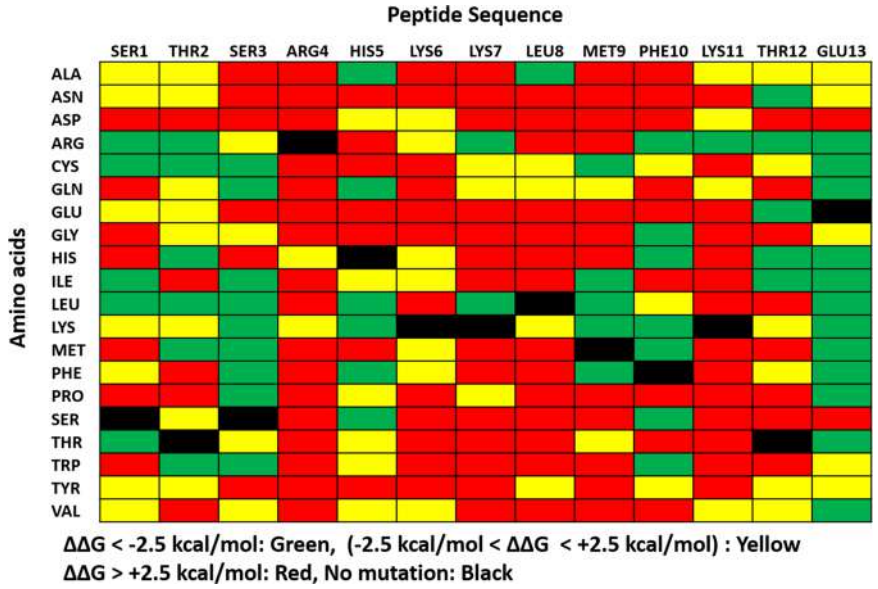

Figure 9. Energetic analysis of the MD simulations of the S100B($\beta\beta$)−mutant peptide complexes. Binding free energy of S100B($\beta\beta$) with each mutant peptide was calculated using the MMPBSA approach (see the Materials and Methods section) using the conformations sampled during the MD simulations of the S100B($\beta\beta$)−mutant peptide complexes. The p53CTD peptide residues are shown along the *X* axis, and the mutated residues are shown along the *Y* axis.

In Silico Optimization of Stapled Peptides. All mutations that showed improved binding affinity were introduced into the three high-affinity stapled peptides (Spep5, Spep9, and Spep10) designed earlier, and in complex with S100B($\beta\beta$) (dimer), were subjected to MD simulations. All of the modified peptides remained stably bound with the S100B($\beta\beta$) (RMSD < 3 Å against the corresponding starting conformation). To quantify the effects of these mutations on the binding affinity, the sampled conformations were subjected to MMPBSA estimates. It was surprising to see that despite all mutant peptides showing increased binding affinity in their unstapled states, they show differential effects on the binding affinity upon stapling. The stapled peptide Spep5 was found to not tolerate any substitution except for two substitutions (S1R and E12R), at the N and C termini of the peptide (Figure 10). Stapled peptide Spep9 was also found to be less tolerant to these substitutions except for three mutations (S1R, T2R, and T12R) that are also located at the N and C termini of the peptides (Figure 10). The peptide Spep10 tolerates several mutations including the introduction of positively charged residues at the termini (Figure 10).

Design of p53CTD-Based Molecular Probes for the Identification of the Biomarker. In addition to their role in the progression of cancer, upregulated levels of S100B($\beta\beta$) are also used as a prognostic indicator, at least for malignant melanoma (MM). As with many cancers, survival from MM is most promising when it is detected early; hence, the development of useful biomarkers for detection and more recently for personalized medicine approaches is an area of intense activity. We take our strongest binding stapled peptide (Spep9_T12R) and model it in conjugation with two imaging agents, 1,4,7,10-tetraazacyclododecane-1,4,7,10-tetraacetic acid (DOTA) and carboxyfluorescein (FAM). Using the decomposition and alanine scanning data generated, we identified the N terminal of the peptide as a potential site for the incorporation of the imaging agents. To investigate whether the addition of a probe at this position interferes with the binding of the peptide to S100B($\beta\beta$), we modeled the

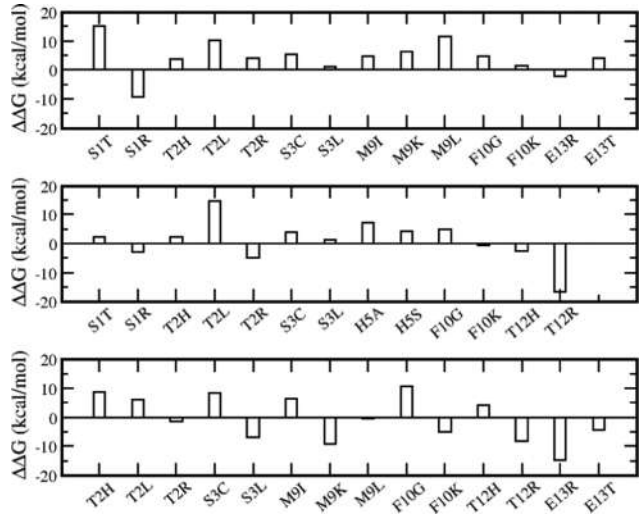

Figure 10. Energetic analysis of the MD simulations of the S100B($\beta\beta$)−stapled (mutant) peptide complexes. Binding free energy of S100B($\beta\beta$) with each mutant stapled peptide was calculated using the MMPBSA approach (see the Materials and Methods section) using conformations sampled during the MD simulations of the complexes. Data is only shown for three peptides as these are the binders with the most favorable computed binding energies (Spep5, top; Spep9, middle; and Spep10, bottom).

S100B($\beta\beta$)−p53CTD:DOTA and S100B($\beta\beta$)−p53CTD:FAM complexes and subjected them to MD simulations (Figure 11). During the simulations, the p53CTD:DOTA/FAM remain bound with RMSD of the bound peptide and S100B($\beta\beta$) within 6 and 4 Å, respectively. The DOTA/FAM moieties do not interfere with the bound peptide, with all of the critical interactions between the unlabeled stapled peptide and S100B($\beta\beta$) retained during the simulations, and similar binding energies (Figure 11) were observed for the DOTA/FAM-labeled and unlabeled peptides.

DOI: 10.1021/acsomega.9b00097
ACS Omega 2019, 4, 5335−5344

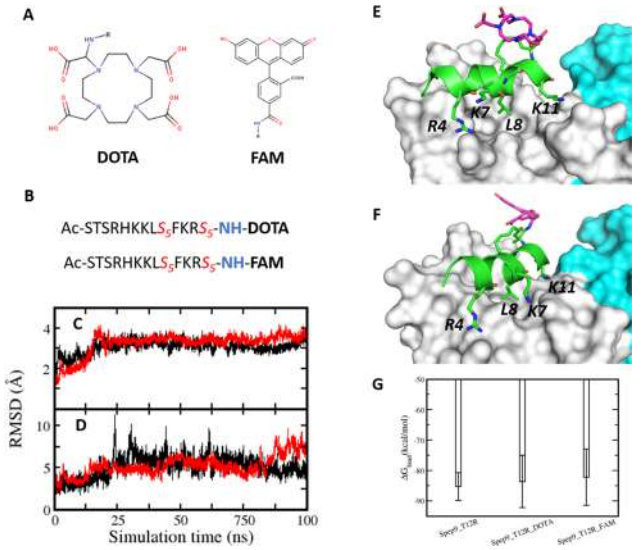

Figure 11. (A) Chemical structure of DOTA and FAM used in this study. (B) Sequence of DOTA and FAM-conjugated stapled peptides. Root-mean-square deviation (RMSD) of (C) S100B($\beta\beta$) and (D) DOTA (black) and FAM-conjugated (red) stapled peptides bound to S100B($\beta\beta$). MD snapshot of (E) S100B($\beta\beta$)−DOTA and (F) S100B($\beta\beta$)−FAM-conjugated stapled peptide complexes. (G) Binding free energies of S100B($\beta\beta$) with the unlabeled stapled peptide (Spep9_T12R), DOTA, and the FAM-labeled stapled peptide (Spep9_T12R) were calculated using the MMPBSA approach.

DISCUSSION

Peptides and peptidomimetics are increasingly being shown to be efficient inhibitors of PPIs. Chemical modifications of the peptides such as stapling have been used to successfully improve conformational stability, improve stability against proteolysis, and enhance cellular entry. Using the solution structure of C terminus of p53 complexed to S100B($\beta\beta$),[47] we designed 15 stapled peptides. The peptides displayed varying helicities (ranging from 17 to 46%) in their free states, but maintained high helicity while in complex with S100B($\beta\beta$), and displayed differential binding affinities with S100B($\beta\beta$). Most of the peptides showed improved binding with S100B($\beta\beta$), although no correlation between the helicity of the free peptide and its binding affinity for S100B($\beta\beta$) was observed. There have been other reports also demonstrating a lack of correlation between helicity of a free stapled peptide and its affinity for its target.[49] To further optimize the binding affinity, we carried out in silico mutation scan by substituting each and every position/residue of the linear peptide with other 19 amino acids using the "Parasol" method.[52] Our in silico scan revealed several positions that favored substitutions (improvements in affinity), especially the residues at the N and C termini that favored positively charged residues; residues that are involved in packing interactions with the S100B($\beta\beta$) are less tolerant to substitutions, as expected. We then used this information to optimize the stapled peptides by introducing the mutations that improved binding in the unstapled peptides. Surprisingly, not all mutations are tolerated in the context of staple linkers, except the ones at the N and C termini that resulted in improved binding. This suggests that the mutations in the unstapled peptides are not transferable to the stapled peptides, and the latter probably needs separate optimization. It is likely that each stapled peptide requires a separate optimization; this is currently being explored. S100B($\beta\beta$) is also a clinically validated biomarker in MM, thus inspiring us to explore the possibility of using the stapled peptides as probes that could be used for the detection of S100B($\beta\beta$). We took Spep9_T12R, the stapled peptide with the highest computed affinity, and identified positions that would tolerate the introduction of chemical labels DOTA and FAM, two widely used imaging agents.

The linear p53CTD peptides (residues 367−388) binds with affinity in the micromolar range (K_d < 23.5 μM).[17] Most stapled peptides designed in this study display improved binding than their linear counterparts (some bind less tightly), and we speculate that the best binder will bind with K_d in the nanomolar range. However, their in vivo stability and cell permeability followed by functional activity will determine their therapeutic validity and these aspects are beyond the scope of the current study. In summary, we have designed several stapled peptides, with improved affinity for S100B($\beta\beta$). These peptides have the potential to abrogate the complexation between the C terminus of p53 and S100B($\beta\beta$) and could serve as good starting points for further development as therapeutic activators of p53.

MATERIALS AND METHODS

System Preparation. In the experimental structure of the p53CTD−S100B($\beta\beta$) complex (PDB ID: 1DT7), S100B($\beta\beta$) exists as a homodimer with a 22-mer fragment (residues 367−388) of p53CTD bound to each unit of S100B($\beta\beta$).[47] We used only one peptide bound with the S100B($\beta\beta$) dimer in the current study. The region 377−388 of the peptide was used as the remaining peptide does not interact with S100B($\beta\beta$).

MD Simulations. MD simulations were carried out with the p53CTD−S100B($\beta\beta$) complex, apo p53CTD, and apo-S100B($\beta\beta$). The apo-S100B($\beta\beta$) refers to S100B($\beta\beta$) bound to calcium ions. This was extracted from the NMR structure (PDB ID: 1DT7), which is a complex of S100($\beta\beta$)−calcium−p53 peptide; the p53 peptide is from the C-terminal region of p53. Since we are designing stapled peptides to displace the wild-type peptide from S100B($\beta\beta$), we chose this complex state because we assume that the stapled peptides (derived from the wild-type p53 in its bound state) will bind to the same region of S100B($\beta\beta$) as the wild-type peptide, without any large conformational changes. In each structure, the N and C termini of the p53CTD fragment were capped with acetyl and *N*-methyl amide groups, respectively. Hydrogen atoms were added to the experimental structures using the xleap module of the Amber16 package.[53] The peptide-binding site contains a few titratable residues; hence, we computed the pK_a of titratable amino acids using PDB2PQR.[54] Only two amino acids, Glu31 and Glu39, were predicted to be unionized at the physiological pH. Hence, we decided to carry out a simulation of the protein with both these amino acids protonated and bound to the wild-type peptide and separately to the tightest binding stapled peptide. These amino acids are >20 Å from the peptides and hence are not expected to affect the binding energetics of the peptides and this is what we found (more details in the Supporting Information); hence, we focused on the system without modifying these two amino acids. All of the systems were neutralized by the addition of counterions. The neutralized systems were solvated with TIP3P[55] water molecules to form a truncated octahedral box with at least 10 Å separating the solute atoms and the edges of the box. MD simulations were carried out with the Sander module of the Amber16 package in combination with the ff14SB force field.[56]

DOI: 10.1021/acsomega.9b00097
ACS Omega 2019, 4, 5335−5344

All of the systems were first subjected to 1000 steps of energy minimization. This was followed by MD simulations, for which the protein was initially harmonically restrained (25 kcal mol Å^2) to the energy minimized coordinates, and the system was heated up to 300 K in steps of 100 K followed by gradual removal of the positional restraints, and a 1 ns unrestrained equilibration at 300 K was carried out. The resulting system was used for MD simulations. Production runs were carried out for 100 ns in triplicates. In addition to MD, both the linear peptide and stapled peptide fragments were subjected to biasing potential replica-exchange molecular dynamics (BP-REMD)[57,58] simulations to enhance the conformational sampling. Biasing potential REMD[57,58] is a Hamiltonian-based REMD (HREMD) with conformational sampling enhanced using a specifically designed dihedral potential.[57,58] In a BP-REMD simulation, different biasing potential levels are applied in each replica (one reference replica run is carried out without any biasing potential) and replica exchanges between neighboring biasing levels were attempted every 1000 MD steps and accepted or rejected according to a Metropolis criterion. The BP-REMD simulations were carried out at 300 K with eight replicas for 50 ns. Parameters for staple linkers were used as described in our previous work.[59]

In Silico Amino Acid Scan Using Parasol. The Parasol protocol[52] was employed in the generation of the mutants. Only mutations between similar enough pairs of amino acids are allowed by the method: for example, isoleucine cannot be mutated to alanine directly but must go through a valine intermediate. For each type of residue, a series of mutations were devised to minimize the number of total simulations and intermediates. Each mutation, in turn, is executed in 11 steps whereby the atoms are transformed, and at each step, MD simulations of 500 steps with a 1 fs time step (5 ps) are carried out, thus totaling 55 ps for each simulation. Finally, each mutant peptide in complex with S100B($\beta\beta$) was subjected to production runs of 100 ns in triplicates.

The parameterization of the DOTA and FAM (imaging agents) was carried using the program NWCHEM,[60] which was used to carry out first a quantum mechanical optimization of the structure and then RESP fitting to generate the charges. Hartree−Fock was used as the method and 6-31g* as the basis set for all the atoms. Both species were parameterized with a cap, whose charges were constrained to be the charges in ff14SB.[56] Chemically equivalent atoms (such as hydrogens attached to the same carbon) were constrained to have the same charge. These imaging agents (DOTA, FAM) were covalently linked to the peptide backbone at the C terminus of the peptides. Production runs of peptide probe−S100B($\beta\beta$) complexes were carried out for 100 ns in triplicates.

Binding Energy Calculations. Molecular mechanics Poisson−Boltzmann surface area (MMPBSA) methods were used for the calculation of binding free energies between the peptides and their partner proteins.[50,51] A total of 250 conformations extracted from the last 50 ns of the simulations were used for the binding energy calculations. Entropy calculations are computationally intensive and do not converge easily and hence are ignored.

Visual molecular dynamics[61] and Pymol[62] were used for visualization of trajectories and preparation of figures, respectively.

■ ASSOCIATED CONTENT

Supporting Information

The Supporting Information is available free of charge on the ACS Publications website at DOI: 10.1021/acsomega.9b00097.

Conformations of p53CTD-bound (green) S100B($\beta\beta$) (Figure S1); root-mean-square deviation (RMSD) of S100B($\beta\beta$) in the bound state (Figure S2); root-mean-square deviation (RMSD) of stapled peptides in bound states (Figure S3) (PDF)

■ AUTHOR INFORMATION

Corresponding Authors

*E-mail: raghavk@bii.a-star.edu.sg. Tel: +65 6478 8353. Fax: +65 6478 9048 (S.K.).

*E-mail: chandra@bii.a-star.edu.sg. Tel: +65 6478 8273. Fax: +65 6478 9048 (C.S.V.).

ORCID

Srinivasaraghavan Kannan: 0000-0002-9539-5249

Chandra S. Verma: 0000-0003-0733-9798

Notes

The authors declare no competing financial interest.

■ ACKNOWLEDGMENTS

The authors thank A*STAR for support; S.K. is partly supported by an IAF-PP grant H18/01/a0/015 from A*STAR/NRF/EDB, Singapore. P.A. is funded by an IAF-PP grant H17/01/a0/101 from A*STAR/NRF/EDB, Singapore. The authors thank National Super Computing Centre (NSCC), Singapore for computing facilities

■ REFERENCES

(1) Kligman, D.; Hilt, D. C. The S100 protein family. *Trends Biochem. Sci.* **1988**, *13*, 437−443.

(2) Marenholz, I.; Heizmann, C. W.; Fritz, G. S100 proteins in mouse and man: from evolution to function and pathology (including an update of the nomenclature). *Biochem. Biophys. Res. Commun.* **2004**, *322*, 1111−1122.

(3) Donato, R. S100: a multigenic family of calcium-modulated proteins of the EF-hand type with intracellular and extracellular functional roles. *Int. J. Biochem. Cell Biol.* **2001**, *33*, 637−668.

(4) Donato, R. Perspectives in S-100 protein biology. Review article. *Cell Calcium* **1991**, *12*, 713−726.

(5) Zimmer, D. B.; Cornwall, E. H.; Landar, A.; Song, W. The S100 protein family: history, function, and expression. *Brain Res. Bull.* **1995**, *37*, 417−429.

(6) Castets, F.; Griffin, W. S.; Marks, A.; Van Eldik, L. J. Transcriptional regulation of the human S100 beta gene. *Brain Res. Mol. Brain Res.* **1997**, *46*, 208−216.

(7) Drohat, A. C.; Baldisseri, D. M.; Rustandi, R. R.; Weber, D. J. Solution structure of calcium-bound rat S100B($\beta\beta$) as determined by nuclear magnetic resonance spectroscopy. *Biochemistry* **1998**, *37*, 2729−2740.

(8) Drohat, A. C.; Nenortas, E.; Beckett, D.; Weber, D. J. Oligomerization state of S100B($\beta\beta$) at nanomolar concentration determined by large-zone analytical gel filtration chromatography. *Protein Sci.* **1997**, *6*, 1577−1582.

(9) Amburgey, J. C.; et al. ^{1}H, ^{13}C, ^{15}N NMR assignments and solution secondary structure of rat Apo-S100b. *J. Biomol. NMR* **1995**, *6*, 171−179.

(10) Drohat, A. C.; et al. Solution structure of rat apo-S100($\beta\beta$) as determined by NMR spectroscopy. *Biochemistry* **1996**, *35*, 11577−11588.

DOI: 10.1021/acsomega.9b00097
ACS Omega 2019, 4, 5335−5344

(11) Drohat, A. C.; Tjandra, N.; Baldisseri, D. M.; Weber, D. J. The use of dipolar couplings for determining the solution structure of rat apo-S100B($\beta\beta$). *Protein Sci.* **1999**, *8*, 800−809.
(12) Kilby, P. M.; Van Eldik, L. J.; Roberts, G. C. K. The solution structure of the bovine S100B protein dimer in the calcium-free state. *Structure* **1996**, *4*, 1041−1052.
(13) Donato, R.; et al. S100B's double life: intracellular regulator and extracellular signal. *Biochim. Biophys. Acta, Mol. Cell Res.* **2009**, *1793*, 1008−1022.
(14) Riuzzi, F.; Sorci, G.; Donato, R. S100B stimulates myoblast proliferation and inhibits myoblast differentiation by independently stimulating ERK1/2 and inhibiting p38 MAPK. *J. Cell Physiol.* **2006**, *207*, 461−470.
(15) Arcuri, C.; Bianchi, R.; Brozzi, F.; Donato, R. S100B increases proliferation in PC12 neuronal cells and reduces their responsiveness to nerve growth factor via Akt activation. *J. Biol. Chem.* **2005**, *280*, 4402−4414.
(16) Harpio, R.; Einarsson, R. S100 proteins as cancer biomarkers with focus on S100B in malignant melanoma. *Clin. Biochem.* **2004**, *37*, 512−518.
(17) Rustandi, R. R.; Drohat, A. C.; Baldisseri, D. M.; Wilder, P. T.; Weber, D. J. The Ca(2+)-dependent interaction of S100B($\beta\beta$) with a peptide derived from p53. *Biochemistry* **1998**, *37*, 1951−1960.
(18) Lin, J.; et al. Inhibition of p53 transcriptional activity by the S100B calcium-binding protein. *J. Biol. Chem.* **2001**, *276*, 35037−35041.
(19) Wilder, P. T.; Rustandi, R. R.; Drohat, A. C.; Weber, D. J. S100B ($\beta\beta$) inhibits the protein kinase C-dependent phosphorylation of a peptide derived from p53 in a Ca^{2+}-dependent manner. *Protein Sci.* **1998**, *7*, 794−798.
(20) Baudier, J.; Delphin, C.; Grunwald, D.; Khochbin, S.; Lawrence, J. J. Characterization of the tumor suppressor protein p53 as a protein kinase C substrate and a S100b-binding protein. *Proc. Natl Acad. Sci. U.S.A.* **1992**, *89*, 11627−11631.
(21) Lin, J.; Yang, Q.; Wilder, P. T.; Carrier, F.; Weber, D. J. The calcium-binding protein S100B down-regulates p53 and apoptosis in malignant melanoma. *J. Biol. Chem.* **2010**, *285*, 27487−27498.
(22) Lin, J.; et al. Inhibiting S100B restores p53 levels in primary malignant melanoma cancer cells. *J. Biol. Chem.* **2004**, *279*, 34071−34077.
(23) Markowitz, J.; et al. Identification and characterization of small molecule inhibitors of the calcium-dependent S100B-p53 tumor suppressor interaction. *J. Med. Chem.* **2004**, *47*, 5085−5093.
(24) Hartman, K. G.; McKnight, L. E.; Liriano, M. A.; Weber, D. J. The evolution of S100B inhibitors for the treatment of malignant melanoma. *Future Med. Chem.* **2013**, *5*, 97−109.
(25) Hussein, M. R.; Haemel, A. K.; Wood, G. S. p53-related pathways and the molecular pathogenesis of melanoma. *Eur. J. Cancer Prev.* **2003**, *12*, 93−100.
(26) Jochemsen, A. G. Reactivation of p53 as therapeutic intervention for malignant melanoma. *Curr. Opin. Oncol.* **2014**, *26*, 114−119.
(27) Zimmer, D. B.; Lapidus, R. G.; Weber, D. J. In vivo screening of S100B inhibitors for melanoma therapy. *Methods Mol. Biol.* **2013**, *963*, 303−317.
(28) Smith, J.; et al. The effect of pentamidine on melanoma ex vivo. *Anti-Cancer Drugs* **2010**, *21*, 181−185.
(29) Charpentier, T. H.; et al. Divalent metal ion complexes of S100B in the absence and presence of pentamidine. *J. Mol. Biol.* **2008**, *382*, 56−73.
(30) Briceland, L. L.; Bailie, G. R. Pentamidine-associated nephrotoxicity and hyperkalemia in patients with AIDS. *DICP, Ann. Pharmacother.* **1991**, *25*, 1171−1174.
(31) Edwards, K. J.; Jenkins, T. C.; Neidle, S. Crystal structure of a pentamidine-oligonucleotide complex: implications for DNA-binding properties. *Biochemistry* **1992**, *31*, 7104−7109.
(32) Pathak, M. K.; et al. Pentamidine is an inhibitor of PRL phosphatases with anticancer activity. *Mol. Cancer. Ther.* **2002**, *1*, 1255−1264.
(33) McKnight, L. E.; et al. Structure-Based Discovery of a Novel Pentamidine-Related Inhibitor of the Calcium-Binding Protein S100B. *ACS. Med. Chem. Lett.* **2012**, *3*, 975−979.
(34) Cavalier, M. C.; et al. Small Molecule Inhibitors of Ca2+-S100B Reveal Two Protein Conformations. *J. Med. Chem.* **2016**, *59*, 592−608.
(35) Cavalier, M. C.; et al. Covalent small molecule inhibitors of Ca(2+)-bound S100B. *Biochemistry* **2014**, *53*, 6628−6640.
(36) Bakail, M.; Ochsenbein, F. Targeting protein−protein interactions, a wide open field for drug design. *C. R. Chim.* **2016**, *19*, 19−27.
(37) Arkin, M. R.; Tang, Y.; Wells, J. A. Small-molecule inhibitors of protein-protein interactions: progressing towards the reality. *Chem. Biol.* **2014**, *21*, 1102−1114.
(38) Wójcik, P.; Berlick, L. Peptide-based inhibitors of protein-protein interactions. *Bioorg. Med. Chem. Lett.* **2016**, *26*, 707−713.
(39) Lau, J. L.; Dunn, M. K. Therapeutic peptides: Historical perspectives, current development trends, and future directions. *Bioorg. Med. Chem.* **2018**, *26*, 2700−2707.
(40) Fosgerau, K.; Hoffmann, T. Peptide therapeutics: current status and future directions. *Drug Discovery Today* **2015**, *20*, 122−128.
(41) Walensky, L. D.; Bird, G. H. Hydrocarbon-stapled peptides: principles, practice, and progress. *J. Med. Chem.* **2014**, *57*, 6275−6288.
(42) Henninot, A.; Collins, J. C.; Nuss, J. M. The current state of peptide drug discovery: Back to the future? *J. Med. Chem.* **2018**, *61*, 1382−1414.
(43) Klein, M. Stabilized helical peptides: overview of the technologies and its impact on drug discovery. *Expert Opin. Drug Discovery* **2017**, *12*, 1117−1125.
(44) Sawyer, T. K.; et al. Macrocyclic α helical peptide therapeutic modality: A perspective of learnings and challenges. *Bioorg. Med. Chem.* **2018**, *26*, 2807−2815.
(45) Wiedmann, M. M.; et al. Development of Cell-Permeable, Non-Helical Constrained Peptides to Target a Key Protein−Protein Interaction in Ovarian Cancer. *Angew. Chem., Int. Ed.* **2017**, *56*, 524−529.
(46) Meric-Bernstam, F. M.; et al. Phase I trial of a novel stapled peptide ALRN-6924 disrupting MDMX- and MDM2-mediated inhibition of WT p53 in patients with solid tumors and lymphomas. *J. Clin. Oncol.* **2017**, *35*, 2505.
(47) Rustandi, R. R.; Baldisseri, D. M.; Weber, D. J. Structure of the negative regulatory domain of p53 bound to S100B($\beta\beta$). *Nat. Struct. Biol.* **2000**, *7*, 570−574.
(48) Shahar, O. D.; et al. Acetylation of Lysine 382 and Phosphorylation of Serine 392 in p53 Modulate the Interaction between p53 and MDC1 In Vitro. *PLoS One* **2013**, *8*, No. e78472.
(49) Baek, S.; et al. Structure of the Stapled p53 Peptide Bound to Mdm2. *J. Am. Chem. Soc.* **2012**, *134*, 103−106.
(50) Genheden, S.; Ryde, U. The MM/PBSA and MM/GBSA methods to estimate ligand-binding affinities. *Expert Opin. Drug Discovery* **2015**, *10*, 449−461.
(51) Wang, C.; Greene, D.; Xiao, L.; Qi, R.; Luo, R. Recent Developments and Applications of the MMPBSA Method. *Front. Mol. Biosci.* **2017**, *4*, 87.
(52) Aronica, P. G. A.; Verma, C.; Popovic, B.; Leatherbarrow, R. J.; Gould, I. R. The Parasol Protocol for computational mutagenesis. *Protein Eng., Des. Sel.* **2016**, *29*, 253−261.
(53) Case, D. A. et al. *AMBER 16*; University of California: San Francisco, 2016.
(54) Dolinsky, T. J.; Nielsen, J. E.; McCammon, J. A.; Baker, N. A. PDB2PQR: an automated pipeline for the setup, execution, and analysis of Poisson-Boltzmann electrostatics calculations. *Nucleic Acids Res.* **2004**, *32*, W665−W667.
(55) Jorgensen, W. L.; Chandrasekhar, J.; Madura, J. D.; Impey, R. W.; Klein, M. L. Comparison of simple potential functions for simulating liquid water. *J. Chem. Phys.* **1983**, *79*, 926−935.
(56) Maier, J. A.; et al. ff14SB: Improving the Accuracy of Protein Side Chain and Backbone Parameters from ff99SB. *J. Chem. Theory Comput.* **2015**, *11*, 3696−3713.

DOI: 10.1021/acsomega.9b00097
ACS Omega 2019, 4, 5335−5344

(57) Kannan, S.; Zacharias, M. Enhanced sampling of peptide and protein conformations using replica exchange simulations with a peptide backbone biasing-potential. *Proteins* **2007**, *66*, 697−706.
(58) Ostermeir, K.; Zacharias, M. Hamiltonian replica-exchange simulations with adaptive biasing of peptide backbone and side chain dihedral angles. *J. Comput. Chem.* **2014**, *35*, 150−158.
(59) Tan, Y. S.; et al. Benzene Probes in Molecular Dynamics Simulations Reveal Novel Binding Sites for Ligand Design. *J. Phys. Chem. Lett.* **2016**, *7*, 3452−3457.
(60) Valiev, M.; et al. NWChem: A comprehensive and scalable open-source solution for large scale molecular simulations. *Comput. Phys. Commun.* **2010**, *181*, 1477−1489.
(61) Humphrey, W.; Dalke, A.; Schulten, K. VMD—visual molecular dynamics. *J. Mol. Graphics* **1996**, *14*, 33−38.
(62) De Lano, W. *The PyMOL Molecular Graphics System*; De Lano Scientific: San Carlos, CA, 2002.

DOI: 10.1021/acsomega.9b00097
ACS Omega 2019, 4, 5335−5344